

Scaling theory of critical strain-stiffening in athermal biopolymer networks

Edan Lerner*

*Institute for Theoretical Physics, University of Amsterdam,
Science Park 904, 1098 XH Amsterdam, the Netherlands*

Eran Bouchbinder†

Chemical and Biological Physics Department, Weizmann Institute of Science, Rehovot 7610001, Israel

Athermal biopolymer networks are disordered fibrous biomaterials abundant in living cells and tissues that feature strong rigidity scale separation between the bending and stretching response of the constituent fibers. Such networks — that are generically underconstrained in terms of their degree of connectivity — undergo a dramatic macroscopic stiffening transition when subjected to sufficiently large external strains, which in turn plays major roles in determining the mechanical stability and functionality of living systems. We present a complete scaling theory of the critical strain-stiffened state in terms of the small ratio between fiber bending and stretching/compression rigidities. We show that the small bending forces may be viewed as an isotropic singular perturbation applied to the stiff anisotropic backbone corresponding to fibers' stretching/compression. The critical state features quartic anharmonicity, from which a set of nonlinear scaling relations for various fundamental biophysical quantities are derived. These results, which are validated by highly accurate numerical simulations, are then used to derive scaling predictions for the macroscopic elastic modulus beyond the critical state, revealing a previously unidentified characteristic strain scale. We thus provide a comprehensive understanding of the strain-stiffening transition in athermal biopolymer networks.

I. INTRODUCTION

Athermal biopolymer fibrous networks, such as collagen and fibrin networks, play crucial roles in determining the mechanical stability and functionality of individual cells and tissues [1–3]. This class of disordered biological materials, in which thermal fluctuations and entropic effects are negligible, is characterized by two generic features; first, the resistance of the constituent fibers to elongation (stretching) and shortening (compression) is much larger than to bending, i.e. these networks exhibit strong rigidity/stiffness scale separation. Second, the degree of connectivity of the fibers, i.e. the average number of fibers per network's node, is small such that the network is sub-isostatic [4]. That is, such materials are underconstrained, implying that in the absence of any bending resistance of the fibers, the network would possess *floppy* (*zero*) *modes*, which are nontrivial, collective deformation modes that do not involve any stretching or compression of fibers, and hence no energetic cost [5]. These two generic features endow athermal biopolymer fibrous networks with intriguing universal properties, which are of both practical and fundamental importance.

The two aforementioned properties of athermal biopolymer fibrous networks are quantified by the dimensionless ratio $\kappa \ll 1$ between fibers' bending and stretching/compression stiffnesses, and by the average connectivity $z < z_c$, where $z_c = 2d$ (d is the space dimension) is the Maxwell rigidity criterion for $\kappa=0$ [6]. A remarkable property of biopolymer fibrous networks is that they

undergo dramatic macroscopic stiffening transition when subjected to external strains. In particular, an initially undeformed network that features a vanishing shear modulus $G=0$ for $\kappa=0$ and $z < z_c$ (cf. Fig. 1a) undergoes a sharp stiffening transition as its shear strain γ attains a critical value γ_c , upon which G features a jump discontinuity, attaining a finite value $G(\gamma_c, \kappa=0)$ [7–9]. This strain-stiffening transition is associated with the emergence of a special internal state, commonly termed a state-of-self-stress (SSS, cf. Fig. 1b), which corresponds to a set of putative stretching or compressive forces in the fibers that exactly balance each other on the network's nodes [9–11].

Substantial experimental, computational and theoretical effort has been made in order to characterize and understand the strain-stiffening transition of athermal biopolymer fibrous networks [1–4, 7–16]. Here, we first develop a complete scaling theory of the critical strain-stiffened state. This is achieved by conceptualizing the entire network as composed of two interacting sub-networks; a stiff underconstrained sub-network at its sharply defined critical state $\gamma = \gamma_c$ and a soft sub-network of a characteristic dimensionless stiffness $\kappa \ll 1$, where the latter is treated as a perturbation on top of the former, see Fig. 1c. This framework allows to derive a set of nonlinear scaling relations for all basic quantities that characterize the critical state, which are verified through highly accurate numerical simulations. We then go beyond the critical state, deriving scaling predictions for $G(\gamma, \kappa)$ away from γ_c , which reveal a previously unidentified characteristic strain scale in athermal biopolymer fibrous networks.

* e.lerner@uva.nl

† eran.bouchbinder@weizmann.ac.il

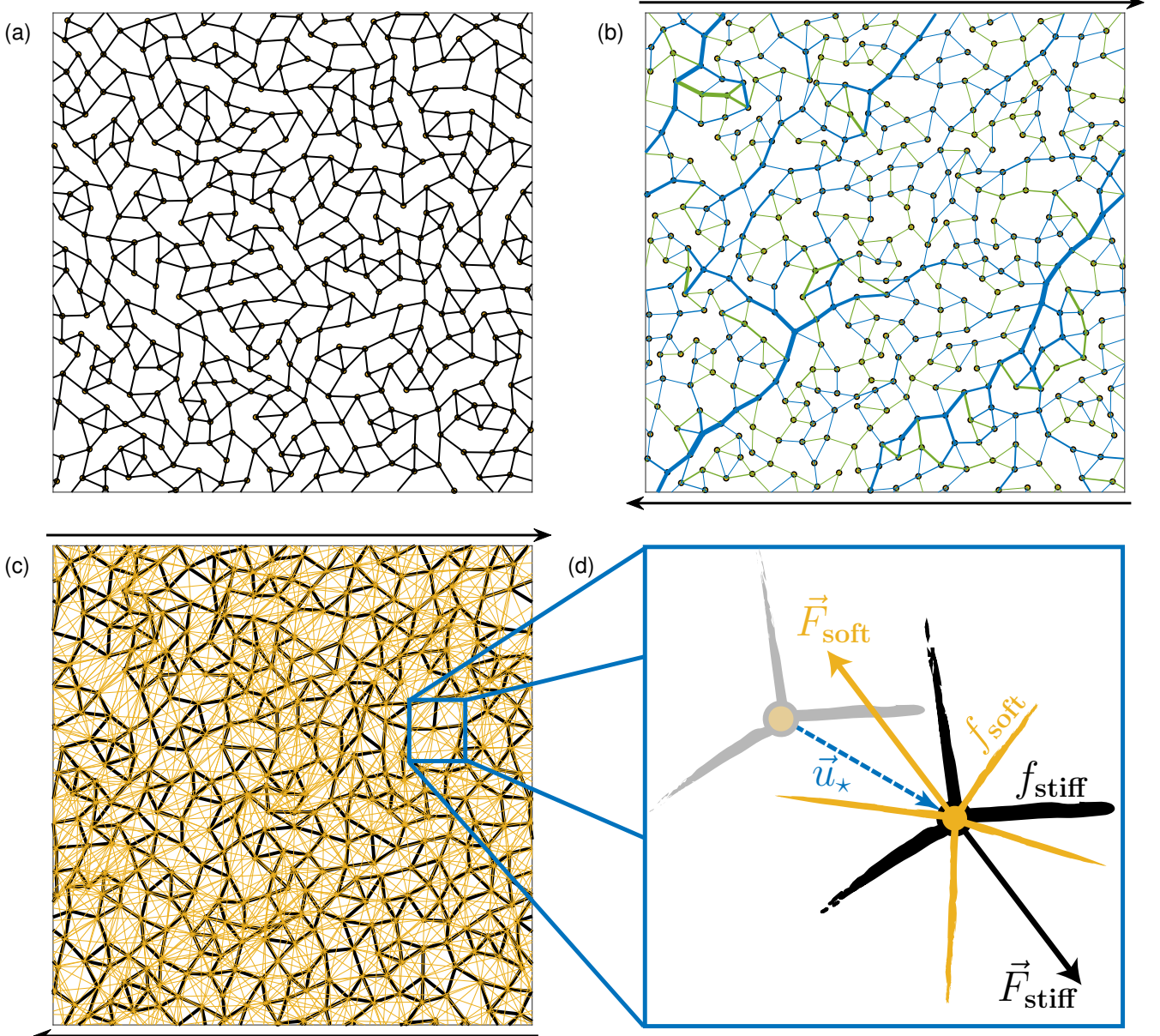


FIG. 1. **An example of a model of a strain-stiffened athermal biopolymer network obtained in a numerical simulation.** (a) An example of the isotropic edge-diluted, disordered floppy networks used in this work, here with $N = 400$ nodes and connectivity of $z = 3.8$ edges per node. (b) The same network shown in (a), after being deformed to the strain-stiffening point. The thickness of the edges represents components of the state-of-self-stress that emerges at the strain-stiffening point, that endows the floppy network with a finite shear modulus [17]. Blue (green) edges mark stretching (compression) forces. (c) An illustration of the two-step procedure aimed at mimicking strain-stiffened fibrous networks in the presence of bending forces. Black edges represent stiff springs of stiffness k (taken to be unit), while yellow edges represent soft springs with stiffness $\kappa \ll 1$ (mimicking bending). (d) Illustration of the force-balance (see text for the definition of the various symbols) between the stiff and soft sub-networks after the introduction of the soft sub-network, followed by node displacement \mathbf{u}_* (dashed arrow).

II. RESULTS

Scaling theory of the critical state. Consider first the stiff, underconstrained sub-network in the absence of strain, see Fig. 1a. Being sub-isostatic, this sub-network features floppy (zero) modes, i.e. modes that

can be deformed without any energetic cost. As a shear strain γ is applied at a given direction, the system self-organizes anisotropically to give rise to the SSS at $\gamma = \gamma_c$, cf. Fig. 1b. There exist, however, an extensive number of zero modes that are not coupled to the applied strain and remain floppy at $\gamma = \gamma_c$. In more formal terms, one can show that floppy modes are orthogonal to the ap-

plied shear strain [18]. Consider then adding the soft sub-network to the stiff one, where the two sub-networks interact at the network's nodes, see Fig. 1c. The soft sub-network may be regarded as a perturbation applied to the stiff one, introducing forces of order κ , i.e. the soft sub-network features a characteristic deformation that is independent of κ (but depends on the average connectivity z) [11].

How would the stiff sub-network respond to the forces introduced to it by the soft sub-network? To address this question, we first note that the soft forces are random and isotropic in nature, and hence will inevitably have projections on the floppy modes of the stiff sub-network, those that persist at γ_c as they are not coupled to the strain. As the floppy modes are energetically cheap to move, one expects them to control the response of the stiff sub-network, for example the node displacements (relative to the node positions prior to the addition of the soft sub-network) of characteristic magnitude u_* , see Fig. 1d.

As the response of the stiff sub-network to the random perturbations introduced by the soft sub-network is expected to be dominated by its floppy modes, its energy $U_{\text{stiff}}(u)$ as function of the node displacement u features vanishing first (mechanical equilibrium) and second (floppy normal modes) derivatives at $u = 0$. Since $u = 0$ is a stable state, a cubic term $\sim u^3$ is also excluded. Hence, we expect $U_{\text{stiff}}(u) \sim u^4$, i.e. that the energy of the stiff sub-network is dominated by quartic anharmonicity, in line with the arguments recently spelled out in [19, 20]. Consequently, the net force applied to the network's nodes by the stiff sub-network follows $F_{\text{stiff}} \sim dU_{\text{stiff}}/du \sim u^3$. As this force balances the imposed soft forces $F_{\text{soft}} \sim \kappa$, i.e. $F_{\text{stiff}} = F_{\text{soft}}$ (cf. Fig. 1d), we predict the network to feature node displacements of characteristic magnitude u_* that scales as

$$u_*(\kappa) \sim \kappa^{1/3}. \quad (1)$$

The basic result in Eq. (1) has immediate implications for the energetics of the system. First, it implies that the energy of the stiff sub-network scales as $U_{\text{stiff}} \sim u_*^4 \sim \kappa^{4/3}$. Since the soft sub-network undergoes κ -independent deformation (of exactly γ_c), its energy scales as $U_{\text{soft}} \sim \kappa$. Taken together, the total energy U of the systems is predicted to scale as

$$U(\kappa) = U_{\text{stiff}}(\kappa) + U_{\text{soft}}(\kappa) \sim U_{\text{soft}}(\kappa) \sim \kappa, \quad (2)$$

since $U_{\text{stiff}} \ll U_{\text{soft}}$ in the limit of small κ . That is, we predict that the total energy of the network is dominated by the energy of the perturbing soft sub-network.

It is natural to consider next the forces in the problem. To that aim, we distinguish between two characteristic forces. The first one corresponds to the net force of magnitude F applied to each node in the network by the two sub-networks (cf. Fig. 1d), $F = F_{\text{stiff}} = F_{\text{soft}}$, where the latter equality follows from mechanical equilibrium, as already invoked above (the *total* net force at

each node obviously vanishes, $F_{\text{total}} = F_{\text{stiff}} - F_{\text{soft}} = 0$). The second one corresponds to the magnitude of the fiber scale force f (cf. Fig. 1d), which includes a contribution from the stiff sub-network f_{stiff} (corresponding to fiber stretching/compression) and a contribution from the soft sub-network f_{soft} (corresponding to fiber bending). Obviously, the vectorial sum of the individual fiber stretching/compression forces equals the net force applied by the stiff sub-network on the network's nodes and likewise the vectorial sum of the individual fiber bending forces equals the corresponding net force applied by the soft sub-network.

With this distinction in mind, we set out to derive a scaling estimate for the eigenvalue λ of the geometrical operator defining the SSS [21], see also Supplementary Information. At the critical γ_c state in the absence of a soft sub-network perturbation, $\kappa = 0$, the geometrical operator associated with the SSS features an identically vanishing eigenvalue, $\lambda = 0$. That means that the eigenvector corresponding to $\lambda = 0$ is interpreted as composed of a set of putative stretching/compression fiber forces that exactly balance on the network's nodes. With the application of a soft sub-network perturbation, $\kappa > 0$, the network node displacements u_* predicted in Eq. (1) emerge and one expects λ to become finite as the $\kappa = 0$ state is distorted. Previous work has shown that λ can be expressed in terms of the ratio F/f as $\lambda \sim (F/f)^2$ [22]. Furthermore, in the Supplementary Information we show that λ increases with the node displacements u_* as $\lambda \sim (F/f)^2 \sim u_*^2$. Using Eq. (1), we then predict

$$\lambda(\kappa) \sim \kappa^{2/3}. \quad (3)$$

The above results can be readily used to obtain a prediction for the fiber scale forces f , and consequently for the stress σ in the network, which satisfies $\sigma \sim f$. First, recall that $F = F_{\text{stiff}} = F_{\text{soft}} \sim \kappa$ and that $f_{\text{soft}} \sim \kappa$. Consequently, Eq. (3) — i.e. $\lambda \sim (F/f)^2 \sim \kappa^{2/3}$ — can be satisfied if f is dominated by the fiber stretching/compression forces, i.e. $f \sim f_{\text{stiff}} \ll F_{\text{stiff}}$. Therefore, we obtain $f_{\text{stiff}} \sim \kappa/\sqrt{\lambda}$, which implies that the network's stress σ satisfies

$$\sigma(\kappa) \sim f_{\text{stiff}}(\kappa) \sim \kappa^{2/3} \quad \text{with} \quad f_{\text{stiff}} \gg f_{\text{soft}}. \quad (4)$$

Quite counter-intuitively and surprisingly, the last relation in Eq. (4) implies that the while the overall network's energy U is dominated by the soft sub-network (corresponding to bending energy), cf. Eq. (2), the overall network's stress σ is dominated by the stiff sub-network (corresponding to stretching/compression forces). This intriguing result is a manifestation of the singular nature of the response of the critical strain-stiffened state to the perturbation introduced by the soft sub-network, to be further discussed below.

The most pronounced macroscopic effect of the strain-stiffening transition in biopolymer fibrous networks is the dramatic increase in the shear modulus G . This stiffening

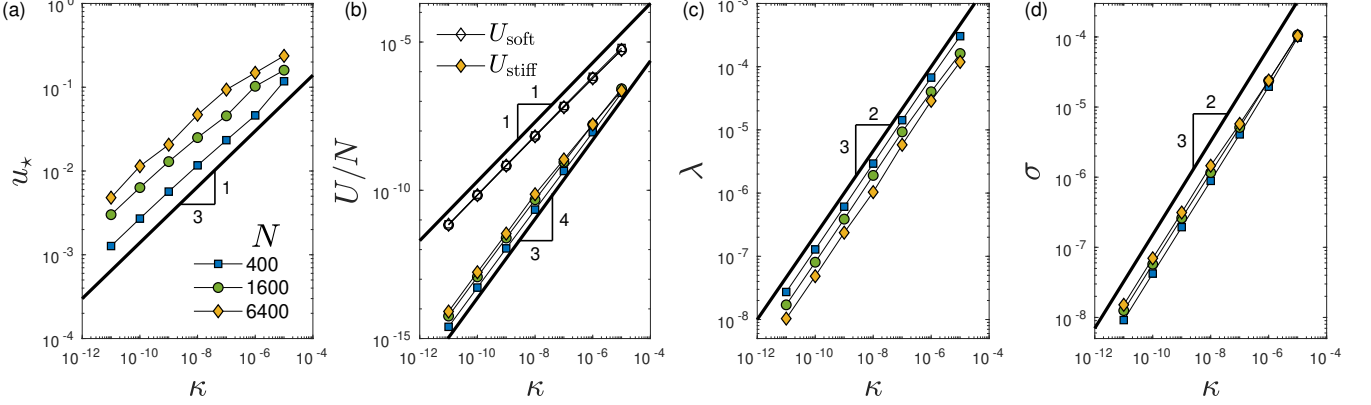


FIG. 2. **High-precision numerical validation of the theoretical predictions at the critical state.** (a) The magnitude u_* of node displacement vectors u_* between the $\kappa = 0$ strain-stiffened state, and the mechanical equilibrium state reached after introducing the soft interactions of stiffness κ (in units of the stiffness of the stiff interactions), cf. Fig. 1a. (b) Energy-per-node U/N of the soft (empty symbols) and stiff (full symbols) sub-networks. (c) The minimal eigenvalue λ of the geometric operator defining the SSS (see Supplementary Information for details), indicating the ratio between the stretching/compression forces in the floppy network's springs, and the resulting net-force on the nodes. (d) The macroscopic shear stress follows σ . All quantities are plotted against κ .

plays important roles in many cellular and tissue-level physiological processes, e.g. it allows the transmission of cellular and tissue forces over large scales, and enables long-range mechanical communication between cells [23]. Our next goal is to understand the properties of G at γ_c .

In view of the finite jump discontinuity experienced by the shear modulus at γ_c , we expect $G(\gamma_c, \kappa)$ to approach a finite value in the $\kappa \rightarrow 0$ limit (see Supplementary Information for additional discussion), i.e. that

$$G(\gamma_c, \kappa \rightarrow 0^+) \sim \kappa^0, \quad (5)$$

even though the $\kappa \rightarrow 0$ limit turns out to be subtle in this context, as discussed below. Next, we aim at calculating the derivative $dG/d\gamma$, evaluated at $\gamma = \gamma_c$, which is nothing but the first nonlinear shear modulus. This observable is sensitive to the presence of low-frequency vibrational modes, and their coupling to external deformation, as pointed out in [24] and explained in the Supplementary Information, where it is shown that

$$\left. \frac{dG(\gamma, \kappa)}{d\gamma} \right|_{\gamma=\gamma_c} \sim \kappa^{-2/3}. \quad (6)$$

Equation (6) predicts that $G(\gamma)$ varies strongly with γ near γ_c and that this variation becomes singular as $\kappa \rightarrow 0$.

The singular perturbation nature of the critical state. As mentioned above, the perturbation introduced by the soft sub-network to the critical strain-stiffened state is of a singular nature. This fundamental point is further highlighted by comparing the response forces f_{stiff} to the imposed force perturbation f_{soft} , i.e. the ratio

$$f_{\text{stiff}}(\kappa)/f_{\text{soft}}(\kappa) \sim \kappa^{-1/3}, \quad (7)$$

which diverges in the $\kappa \rightarrow 0$ limit. That is, the response is infinitely stronger than the perturbation.

In addition, let us consider again the shear modulus G at γ_c . A careful calculation, presented in the Supplementary Information, reveals that the value approached in the $\kappa \rightarrow 0^+$ limit, differs from $G(\gamma_c, \kappa = 0)$, i.e. the value obtained at $\kappa = 0$. It is shown that in fact we have

$$G(\gamma_c, \kappa \rightarrow 0^+) = G(\gamma_c, \kappa = 0) - \Delta G \equiv G(\gamma_c) \quad (8)$$

in the limit $\kappa \rightarrow 0^+$, where $\Delta G > 0$ contains a product of two contributions, one that scales as $\kappa^{-2/3}$ and another as $\kappa^{2/3}$ such that the limit $\kappa \rightarrow 0^+$ is finite. Consequently, Eq. (8) indicates that the limit $\kappa \rightarrow 0^+$ is different from setting $\kappa = 0$, yet again revealing the singular nature of the κ perturbation in the problem.

III. NUMERICAL VALIDATION.

Our next goal is to quantitatively test the predictions of the scaling theory developed above through highly accurate numerical calculations. To this aim, we employ disordered networks of relaxed Hookean springs in two-dimensions ($d=2$, 2D) with mean connectivity of $z=3.8$, see Methods.

We subject our networks to simple shear strain of magnitude γ (see Methods for details); as long as $\gamma < \gamma_c$, the potential energy remains zero (demonstrated in the Supplementary Information). However, at γ_c the system strain-stiffens — it acquires a finite shear modulus. Accurately resolving the critical strain γ_c is difficult from a numerical/computational perspective; the reason is that, at γ_c , the energy in the spring network should be vanishingly small. This means that the actual length of springs is very close to their rest-length. In addition, since we aim at finding a minimum of the potential energy, at which the forces exerted by the springs on the nodes balance

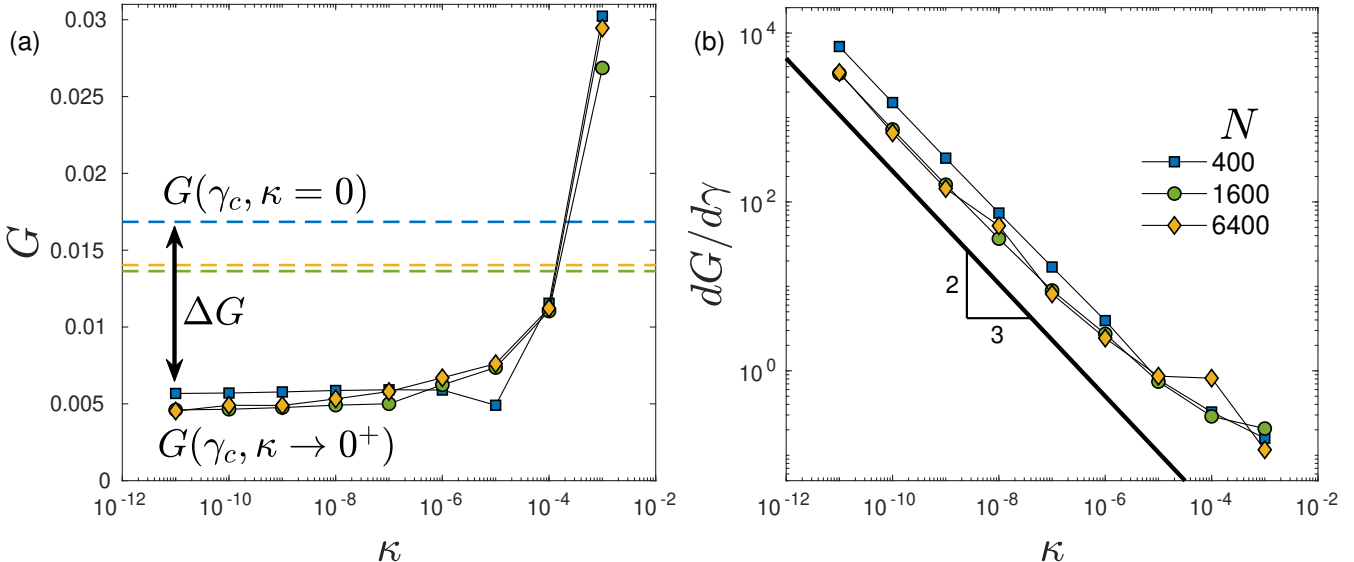


FIG. 3. **High-precision numerical validation of the theoretical predictions for the linear and first nonlinear shear moduli.** (a) The shear modulus G of a strain-stiffened network in the presence of the soft interactions, of stiffness κ . We find that G approaches a constant as $\kappa \rightarrow 0^+$, as predicted (see Eq. (8) and Supplementary Information). The dashed lines indicate the value of the shear modulus when $\kappa = 0$ identically, underlining the singular-perturbative nature of the soft (bending) interactions. (b) The first nonlinear shear modulus $dG/d\gamma$ follows the theoretical prediction $\sim \kappa^{-2/3}$ in Eq. (6).

each other *exactly*, we must resolve the *differences* between the aforementioned differences between the spring lengths and their corresponding rest-lengths.

The computational problem of accurately resolving differences-of-differences of numbers that are very similar to each other — requires employing 128-bit floating point precision numerics. The latter turns out to be essential for probing the physics of the critical strain stiffening point. By employing 128-bit numerics, we are able to generate strain-stiffened networks (i.e. at γ_c) with an energy-per-node of order $10^{-20}k\ell^2$ (see Supplemental Information), where k denotes the spring stiffnesses (shared by all springs) and $\ell \equiv \sqrt{A/N}$ forms the microscopic units of length of our networks of area A .

In order to mimic strain-stiffened networks at finite- κ , we employ a ‘two-step procedure’ as explained in Methods, which involves introducing an additional, soft interaction potential to the critical networks at γ_c , which represents the fibers’ bending energy. The addition of the soft interaction does not alleviate the numerical challenge, at small κ (of order 10^{-10} or lower): as explained above, now the vanishing differences between the forces in the stiff network (which, we reiterate, themselves require resolving the vanishing difference between the springs’ lengths and rest-lengths) need to be balanced by a force of order κ — which becomes challenging for the smallest κ probed in our work.

These aforementioned numerical challenges that force us to resort to 128-bit numerics dramatically limit the size and number of systems one can generate. For this reason, we generated a *single* realization of strain-

stiffened networks for different system sizes N (number of network’s nodes), both at $\kappa = 0$ and at various finite κ (using the two-step procedure), rather than ensembles of systems, as conventionally done. Nevertheless, these single realizations appear sufficient to validate our theoretical predictions, as shown next.

In Fig. 2, we validate the predictions of Eqs. (1)-(4), for our 3 networks of $N = 400, 1600$ and 6400 nodes at $z = 3.8$. Additional details can be found in the figure caption. We find excellent agreement with all scaling predictions. In Fig. 3, we validate the predictions of Eqs. (5)-(6), in addition to demonstrating the singular-perturbative nature of the soft-subsystem and illustrating the observables defined in Eq. (8). Moreover, in Fig. 3 we use κ values as high as $\kappa = 10^{-3}$ in order to highlight the fact that the critical scaling at γ_c for small κ must break down for large enough κ . This is nicely demonstrated in Fig. 3a, where $G(\gamma_c, \kappa)$ reveals a clear deviation from the $G(\gamma_c, \kappa \rightarrow 0^+)$ value with increasing κ .

IV. SCALING THEORY BEYOND THE CRITICAL POINT.

Our next goal is to go beyond the critical point, i.e. to understand the scaling structure of $G(\gamma, \kappa)$ near γ_c using Eqs. (5)-(6). The first step in achieving this goal is to formulate what is the physical meaning of “being near γ_c ”. The latter entails the existence of a characteristic κ -dependent strain scale $\delta\gamma_*(\kappa) > 0$ such that $|\gamma - \gamma_c| \ll \delta\gamma_*(\kappa)$ defines “being near γ_c ”, both below and above

the critical strain γ_c . Consequently, we pose the simplest scaling ansatz of the form

$$G(\gamma, \kappa) \sim \mathcal{F}\left(\frac{\gamma - \gamma_c}{\delta\gamma_*(\kappa)}\right), \quad (9)$$

where $\mathcal{F}(\cdot)$ is a dimensionless scaling function and G is nondimensionalized by k/ℓ . The challenge then is to derive both $\delta\gamma_*(\kappa)$ and $\mathcal{F}(\cdot)$.

Denoting $x \equiv (\gamma - \gamma_c)/\delta\gamma_*(\kappa)$ and taking the derivative of G in Eq. (9) with respect to γ , evaluated at γ_c , we obtain $dG/d\gamma|_{\gamma=\gamma_c} = d\mathcal{F}/dx|_{x=0}[\delta\gamma_*(\kappa)]^{-1}$. To comply with Eq. (6), $d\mathcal{F}/dx|_{x=0}$ has to be finite, i.e. \mathcal{F} varies linearly with x to leading order, and

$$\delta\gamma_*(\kappa) \sim \kappa^{2/3}. \quad (10)$$

Moreover, Eq. (5) implies $\mathcal{F}(x=0) = G(\gamma_c)$ (the latter is defined in Eq. (8)). Consequently, we end up with

$$G(\gamma, \kappa) - G(\gamma_c) \sim \kappa^{-2/3}(\gamma - \gamma_c) \quad \text{for } |\gamma - \gamma_c| \ll \kappa^{2/3}. \quad (11)$$

Equation (10) predicts that the characteristic strain scale $\delta\gamma_*(\kappa)$ vanishes in the limit $\kappa \rightarrow 0$ with a nontrivial exponent. Equation (11) predicts that $G(\gamma, \kappa)$ varies linearly with γ on top of the constant $G(\gamma_c)$, both below and above γ_c . That is, we predict that $G(\gamma, \kappa)$ is regular near γ_c in terms of its variation with the strain γ .

Can the scaling form $G(\gamma, \kappa) \sim \mathcal{F}\left(\frac{\gamma - \gamma_c}{\kappa^{2/3}}\right)$ be used to obtain predictions also at smaller strains γ below the characteristic strain scale, i.e. for $\gamma_c - \gamma \gtrsim \kappa^{2/3}$? Below the strain-stiffening transition, the characteristic scale of G is determined by the soft sub-network, i.e. G has to be linear in κ . The above scaling form then immediately predicts the γ dependence of $G(\gamma, \kappa)$, leading to

$$G(\gamma, \kappa) \sim \kappa(\gamma_c - \gamma)^{-3/2}, \quad (12)$$

i.e. we expect $\mathcal{F}(x) \sim x^{-3/2}$ in this regime below the critical point, in perfect agreement with the arguments and numerical result of Ref. [11]. Equation (12) is expected to hold at an intermediate crossover regime below γ_c , where G significantly increases with γ . As will be shown below, this prediction is consistent with extensive numerical data available in the literature.

At the same time, it is clear that the scaling ansatz $G(\gamma, \kappa) \sim \mathcal{F}\left(\frac{\gamma - \gamma_c}{\kappa^{2/3}}\right)$ cannot hold in other regimes further away from the critical point, as explained in the Supplementary Information. The scaling theory of Eqs. (9)-(12) also implies that previous attempts [4, 15, 16] to describe the strain-stiffening transition using a Widom-like scaling [25] of the form $G(\gamma, \kappa) \sim |\gamma - \gamma_c|^f \mathcal{G}_\pm(\kappa/|\gamma - \gamma_c|^\phi)$, with $f, \phi > 0$ (here \pm corresponds to the strain regimes above and below γ_c , respectively), cannot be strictly valid, as is further discussed in the Supplementary Information.

V. AGREEMENT WITH NUMERICAL RESULTS AVAILABLE IN THE LITERATURE.

As the strain-stiffening transition has been quite extensively studied in the literature using numerical simulations, it would be interesting at this point to test some of our predictions against numerical results available in the literature. Very recently [16], the rheology of fluid-immersed, strain-stiffened networks near γ_c has been numerically studied using overdamped simulations. It has been shown (cf. Eq. 5 and Fig. 3c therein) that the excess viscosity at γ_c scales as $\kappa^{-\xi}$. The excess viscosity is related to the square of the non-affine displacements [22], which we predict to scale as $\sim \kappa^{-2/3}$ (see Supplementary Information). In [16], it was found that $\xi \approx 1.5/2.2 \approx 0.68$, in great quantitative agreement with our prediction.

The scaling theory of Eqs. (9)-(12), and Eq. (10) in particular, predicts the existence of a characteristic strain scale $\delta\gamma_*(\kappa)$ from both sides of γ_c , which shrinks with decreasing κ . Evidence for the existence of such a shrinking strain scale below γ_c is provided in Fig. 1 of [11], where $G(\gamma, \kappa)$ is plotted as a function of γ for various values of κ (note that the parameter varied in that figure is κ^{-1}), and above γ_c in Fig. 5.3. of [8], where the square of the non-affine displacements is plotted as a function of γ for various values of κ . While these figures — reproduced for the sake of completeness in the Supplementary Information — do not allow to extract the functional form of $\delta\gamma_*(\kappa)$ (to be compared with Eq. (10)), they clearly indicate its existence.

The prediction in Eq. (12) is consistent with extensive numerical data available in the literature. In [4, 13, 15], it has been observed that $G(\gamma_c - \gamma)^{-f} \sim \kappa(\gamma_c - \gamma)^{-\phi}$ (i.e. $G \sim \kappa(\gamma_c - \gamma)^{f-\phi}$) with $f - \phi$ close to $-3/2$, below γ_c . Specifically, in [13], $f - \phi \approx 0.53 - 2.0 = -1.47$ (2D undistorted honeycomb lattice, cf. Fig. 4a therein) and $f - \phi \approx 0.63 - 1.9 = -1.27$ (2D undistorted triangular lattice, cf. Fig. 4d therein) have been reported; in [4], $f - \phi \approx 0.75 - 2.1 = -1.35$ (2D triangular lattice, cf. Fig. 2b therein), $f - \phi \approx 0.84 - 2.2 = -1.38$ (2D Mikado network, cf. Fig. 2b therein) and $f - \phi \approx 0.8 - 2.2 = -1.4$ (3D fcc lattice, cf. Fig. 2b therein) have been reported; and in [15], $f - \phi \approx 0.73 - 2.26 = -1.53$ (2D triangular network, cf. Fig. 3a therein) and $f - \phi \approx 0.68 - 2.05 = -1.37$ (2D packing-derived network, cf. Fig. 3b therein) have been reported. These are all in reasonable agreement with our prediction $f - \phi = -3/2 = -1.5$ in Eq. (12).

The observations discussed above provide strong independent support to our scaling theory. Moreover, as these literature calculations involved deforming fibrous networks at finite κ values, their consistency with our predictions also supports the developed framework in which the entire network is viewed as two interacting sub-networks, where the soft (fiber bending) sub-network is treated as a perturbation to the stiff (fiber stretching/compression) sub-network near γ_c (the so-called ‘two-step procedure’). In addition, in [9]

(cf. Fig. 4D therein) and in [8] (cf. Fig. 5.1 therein), $G - G(\gamma_c) \sim (\gamma - \gamma_c)$ has been observed above and close to γ_c for $\kappa = 0$, apparently in agreement with the prediction in Eq. (11). This apparent agreement, however, should be taken with caution as Eq. (11) is valid in the $\kappa \rightarrow 0$ limit (and note the predicted diverging $\kappa^{-2/3}$ prefactor), which may (or may not) differ from its $\kappa = 0$ counterpart in terms of the scaling with γ . Future work should further clarify this point.

VI. DISCUSSION

In this work, we developed a comprehensive scaling theory of the strain-stiffening transition of athermal biopolymer fibrous networks, at and near the critical strain γ_c . Building on the intrinsic stiffness scale separation between fiber bending and stretching/compression, we treated the sub-network of weak bending forces as a random and isotropic perturbation of dimensionless magnitude $\kappa \ll 1$ applied to the anisotropic stiff sub-network at γ_c . With this conceptual framework in mind, we theoretically predicted the dependence of the salient physical quantities in the problem on κ at the critical strain γ_c .

The existence of floppy modes that are uncoupled (orthogonal) to the applied strain have been shown to dominate the stiff sub-network's response to the weak bending forces, which is characterized by quartic anharmonicity, in line with recent theoretical arguments [19, 20]. The κ scaling of the network's node displacements and of its energy at γ_c then follow, cf. Eqs. (1)-(2). Furthermore, analyzing the state-of-self-stress (SSS) and its breakdown in the presence of weak bending forces, as well as the accompanying non-affinity, allowed us to predict the κ scaling of the forces in the problem and of the macroscopic modulus G at γ_c , cf. Eqs. (3)-(6). The structure of the theory highlights the role of κ as a singular perturbation applied to the critical strain-stiffened state, two manifestations of which are discussed in the context of Eqs. (7)-(8)

Numerically testing the set of κ scaling predictions for various physical quantities at γ_c pose a significant challenge and require high-precision numerical simulations. This challenge has been met and led to excellent quantitative agreement with the theoretical predictions. Independent support to the scaling at γ_c is provided by recent numerical results in the literature [16] for the rheology of fluid-immersed, strain-stiffened networks, see discussion above.

With the complete κ scaling theory at γ_c and its numerical validation at hand, we extended the theory beyond the critical state and derived scaling relations for the macroscopic modulus $G(\gamma, \kappa)$ in Eqs. (9)-(12). These scaling relations highlight the existence of a previously unidentified characteristic κ -dependent strain scale $\delta\gamma_*(\kappa)$ near γ_c . Available numerical results in the litera-

ture lend independent support to some of the predictions, which should be further tested in their entirety in future work. Furthermore, the structure of the emerging scaling theory indicates that the Widom-like scaling form assumed in previous work [4, 15] cannot be strictly and self-consistently valid.

The progress made in this work also opens the way for additional future investigations. The most immediate and pressing ones are the substantiation of the predicted strain scale in Eq. (10) and of the linear γ scaling near γ_c according to Eq. (11). In addition, a more thorough quantitative comparison between the two-step procedure (in which a critical γ_c state is supplemented with a $\kappa \ll 1$ soft sub-network) and the continuous straining procedure at $\kappa > 0$ should be performed. Achieving this comparison is a substantial computational challenge for the same reasons spelled out above, i.e. each network realization requires performing thousands of minimization steps of the potential energy with 128-bit precision, which are extremely costly from a running time perspective.

In this work, we did not address spatial aspects of the strain-stiffening transition. Yet, it is conceivable that a characteristic lengthscale that increases with decreasing κ exists in this problem [10, 11]. In this context, it would be interesting to explore finite size effects encountered in computer simulations, which have not been discussed and quantified here (according to Figs. 2-3, these appear to be rather weak). Moreover, the existence of a characteristic lengthscale is expected to be intimately related to the spatial decay of mechanical perturbation throughout the fibrous network, which may have profound implications for cell-cell communication in realistic biopolymer networks.

As discussed above and in the Supplementary Information, the scaling form in Eq. (9) cannot remain valid away from the critical point γ_c , i.e. different scaling relations are expected for $|\gamma - \gamma_c| \gg \delta\gamma_*(\kappa)$. While these scaling relations have been numerically explored [4, 8, 12, 15, 16], theoretically deriving them remains a challenge for future work. Finally, we did not consider in this work possible differences between the effect of applied shear and dilatational strains, and in particular all numerical validation tests were performed under shear strains. It would be interesting to systematically explore dilatational strains in future work.

ACKNOWLEDGMENTS

We thank Gustavo Düring for enlightening discussions that led to this work and Eric Lerner for his assistance with the graphics of Fig. 1. E.L. acknowledges Support from the NWO (Vidi grant no. 680-47-554/3259). E.B. acknowledges support from the Ben May Center for Chemical Theory and Computation and the Harold Perlman Family.

METHODS

A. Preparation of initial isotropic networks.

In order to generate disordered networks of relaxed Hookean springs, we first create packings of harmonic discs — similar to the ones studied e.g. in [26] —, at a packing fraction of 1.0. We then adopt the network of contacts between the harmonic discs to form an initial disordered network of nodes and edges. The edges of these initial random networks are then diluted following the algorithm described in [27], which maintains low fluctuations in the local connectivity of nodes. Edge-dilution is stopped once the network reaches a connectivity (per node) of $z = 3.8$, which resides *below* the Maxwell threshold $z_c = 2d$ [6] (they are thus referred to as *underconstrained* or *floppy* networks). Then, each edge is substituted with a fully relaxed Hookean spring of stiffness k (which is used as the unit of stiffness in the problem). An example of such an edge-diluted disordered network is displayed in Fig. 1a. The resulting disordered floppy networks are then subjected to athermal, quasistatic deformation, which involves repeatedly applying small shear-strain increments, and following each increment with a potential energy minimization [28]. Further technical details are provided in the Supplementary Information.

B. Adding the soft sub-network (representing bending forces).

In order to mimic strain-stiffened networks, whose fibers feature both stretching and bending energies, we add a highly-coordinated network of weak (soft) Hookean springs — of spring stiffness κ (made dimensionless by k) — to the strain-stiffened spring networks, as illustrated in Fig. 1c, and described in detail in the Supplementary Information. Adding the weak interaction introduces net-forces of order κ on the nodes. We then minimize again the potential energy, while including the weak interaction as well. This ‘two-step procedure’ also requires 128-bit numerics, for the same reasons previously spelled out.

C. Observables

All derivatives of the potential energy with respect to strain are calculated with 128-bit precision numerics, using the exact expressions for linear and nonlinear athermal elasticity of disordered solids, see e.g. [29, 30]. The exact expressions used are also provided in the Supplemental Information.

[1] C. Storm, J. J. Pastore, F. C. MacKintosh, T. C. Lubensky, and P. A. Janmey, *Nature* **435**, 191 (2005).

[2] I. Levental, P. C. Georges, and P. A. Janmey, *Soft Matter* **3**, 299 (2007).

[3] C. P. Broedersz and F. C. MacKintosh, *Rev. Mod. Phys.* **86**, 995 (2014).

[4] A. Sharma, A. J. Licup, K. A. Jansen, R. Rens, M. Sheinman, G. H. Koenderink, and F. C. MacKintosh, *Nature Physics* **12**, 584 (2016).

[5] G. Düring, E. Lerner, and M. Wyart, *Soft Matter* **9**, 146 (2013).

[6] J. C. Maxwell, *Philos. Mag.* **27**, 294 (1864).

[7] M. F. J. Vermeulen, A. Bose, C. Storm, and W. G. El lenbroek, *Phys. Rev. E* **96**, 053003 (2017).

[8] R. Rens, *Theory of rigidity transitions in disordered materials* (PhD thesis, University of Amsterdam, the Netherlands, 2019).

[9] M. Merkel, K. Baumgarten, B. P. Tighe, and M. L. Manning, *Proc. Natl. Acad. Sci. U.S.A.* **116**, 6560 (2019).

[10] G. Düring, E. Lerner, and M. Wyart, *Phys. Rev. E* **89**, 022305 (2014).

[11] R. Rens, C. Villarroel, G. Düring, and E. Lerner, *Phys. Rev. E* **98**, 062411 (2018).

[12] A. J. Licup, A. Sharma, and F. C. MacKintosh, *Phys. Rev. E* **93**, 012407 (2016).

[13] R. Rens, M. Vahabi, A. J. Licup, F. C. MacKintosh, and A. Sharma, *J. Phys. Chem. B* **120**, 5831 (2016).

[14] M. Wyart, H. Liang, A. Kabla, and L. Mahadevan, *Phys. Rev. Lett.* **101**, 215501 (2008).

[15] J. L. Shivers, S. Arzash, A. Sharma, and F. C. MacKintosh, *Phys. Rev. Lett.* **122**, 188003 (2019).

[16] J. L. Shivers, A. Sharma, and F. C. MacKintosh, *arXiv preprint arXiv:2203.04891* (2022).

[17] M. Wyart, *Ann. Phys. Fr.* **30**, 1 (2005).

[18] The relevant observable is $\langle \Psi | F_\gamma \rangle$ where $|\Psi\rangle$ represents a floppy mode and $|F_\gamma\rangle$ are the forces on the network’s nodes that arise due to the application of a strain γ . Since in mechanical equilibrium of our floppy networks $|F_\gamma\rangle = \mathcal{S}^T |\partial r / \partial \gamma\rangle$ (see Supplementary Information for details), and floppy modes satisfy $\mathcal{S}|\Psi\rangle = 0$, then it follows that $\langle \Psi | F_\gamma \rangle = 0$.

[19] O. K. Damavandi, V. F. Hagh, C. D. Santangelo, and M. L. Manning, *Phys. Rev. E* **105**, 025003 (2022).

[20] O. K. Damavandi, V. F. Hagh, C. D. Santangelo, and M. L. Manning, *Phys. Rev. E* **105**, 025004 (2022).

[21] E. Lerner, *Eur. Phys. J. E* **41**, 93 (2018).

[22] E. Lerner, G. Düring, and M. Wyart, *Proc. Natl. Acad. Sci. U.S.A.* **109**, 4798 (2012).

[23] S. Goren, Y. Koren, X. Xu, and A. Lesman, *Biophys. J.* **118**, 1152 (2020).

[24] H. G. E. Hentschel, S. Karmakar, E. Lerner, and I. Procaccia, *Phys. Rev. E* **83**, 061101 (2011).

[25] B. Widom, *J. Chem. Phys.* **43**, 3898 (1965).

- [26] E. Lerner, E. DeGiuli, G. During, and M. Wyart, *Soft Matter* **10**, 5085 (2014).
- [27] G. Kapteijns, E. Bouchbinder, and E. Lerner, *Phys. Rev. E* **104**, 035001 (2021).
- [28] E. Bitzek, P. Koskinen, F. Gähler, M. Moseler, and P. Gumbsch, *Phys. Rev. Lett.* **97**, 170201 (2006).
- [29] J. F. Lutsko, *J. Appl. Phys.* **65**, 2991 (1989).
- [30] S. Karmakar, E. Lerner, and I. Procaccia, *Phys. Rev. E* **82**, 026105 (2010).

Supplementary Information —

“Scaling theory of critical strain-stiffening in athermal biopolymer networks”

The goal of this Supplementary Information file is to provide additional technical details regarding the numerical results and the derivation of the scaling predictions presented in the main text.

S-I. THE $\kappa=0$ STRAIN-STIFFENING TRANSITION

To set the stage to the discussion of the strain-stiffening transition in athermal biopolymer fibrous networks, we first consider the $\kappa=0$ case, i.e. a situation in which the constituent fibers do not possess a finite bending rigidity. We consider a simple model of athermal biopolymer networks — a random, underconstrained (hypostatic, having a coordination $z < 2d$ with d denoting the dimension of space) network of Hookean springs of uniform stiffness (that is used at the stiffness scale in the problem), in two dimensions ($d=2$, 2D). Our networks were derived from packings of soft discs, following the algorithm described in [S1]. We deform our networks using an athermal, quasistatic scheme that involves applying small shear-strain increments $\Delta\gamma$ — as small as $\Delta\gamma \sim 10^{-9}$ —, and follow each such incremental deformation by a potential energy minimization [S2]. The stopping criterion for the minimization is: either (i) the typical force f_{stiff} exerted by *individual* springs on the nodes they connect decreases below 10^{-10} (relevant for floppy states with $G=0$), or (ii) the ratio between the typical *net* force F_{stiff} exerted on nodes, to the typical force f_{stiff} exerted by *individual* springs, drops below 10^{-10} (relevant for strain-stiffened states for which $G>0$).

At some critical strain γ_c , the sheared networks undergo a strain-stiffening transition, at which the shear modulus changes discontinuously from $G=0$ at $\gamma < \gamma_c$, to $G \neq 0$ for $\gamma \leq \gamma_c$ [S3–S5]. We employ 128-bit numerics in order to approach the critical point, such that the energy-per-node $U/N \sim 10^{-20}$. This numerical precision is necessary, as motivated in the main text. We present in Fig. S1 the behavior of the energy U (first row), the stress σ (second row) and the shear modulus G (third row) across the transition for the 3 system sizes (quantified by the number of network's nodes N) employed in this work. We also explain therein the notations for $G(\gamma_c, \kappa \rightarrow 0^+)$ and ΔG , used in the main text.

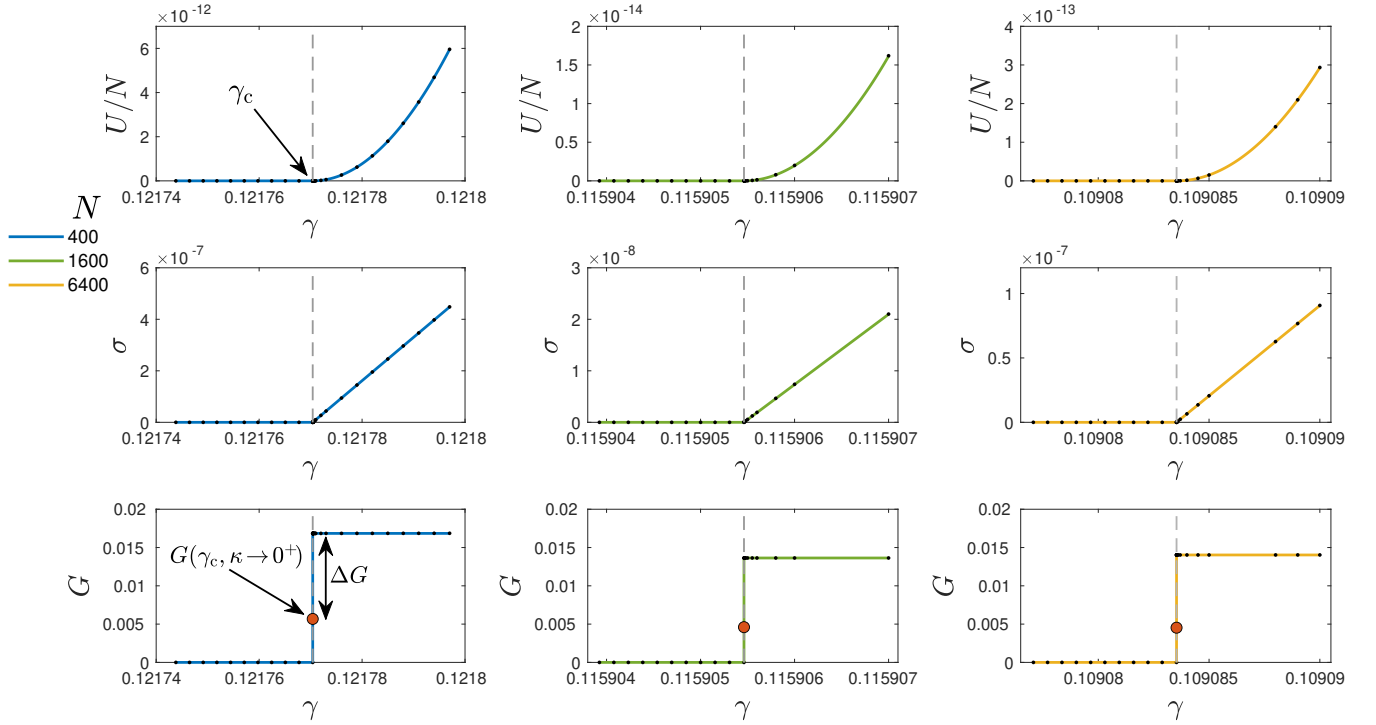


FIG. S1. Overview of the $\kappa=0$ strain-stiffening transition, setting the stage to the $\kappa>0$ situation focused on in this work. The columns correspond to different system sizes as detailed in the legend. The vertical dashed lines mark the critical stiffening strain γ_c . The continuous lines in the top two rows are plotted based on the measurement of $G(\gamma_c, \kappa=0)$, and the black dots are measurements at strains $\gamma \neq \gamma_c$.

S-II. THE TWO-STEP PROCEDURE

In order to mimic networks whose fibers are also endowed with bending rigidity, we add weak interactions to our critical (i.e. at γ_c), strain-stiffened spring networks — of dimensionless stiffness κ as follows:

1. We consider the isotropic floppy ($z < 2d$) network before it has been sheared. We add weak relaxed Hookean springs — of stiffness $\kappa \ll 1$, to all pairs of nodes that are not already connected with a stiff spring, and whose pairwise distance is smaller than a threshold $\approx 2a_0$ where $a_0 \equiv \sqrt{A/N}$ with A denoting the system's area, and N denotes the number of nodes. The mean connectivity of the resulting network of weak springs is about 6, i.e. much larger than the Maxwell threshold of $2d$.
2. We then record the rest-lengths of the relaxed weak springs in the isotropic state, reload the strain stiffened network at γ_c , and assign the weak springs as defined on the isotropic network, to the ($\kappa = 0$) strain-stiffened network. At the latter state, the weak springs no longer reside at their rest-lengths, and consequently they exert a force of order κ on the strain-stiffened network's nodes. The total potential energy $U = U_{\text{stiff}} + U_{\text{weak}}$ is then minimized using 128-bit numerics. The stopping criterion for the minimization at finite κ is that the typical net force is less than 10^{-10} of the typical force in the *weak* springs.

This ‘two-step procedure’ is illustrated in Fig. 1 of the main text. In Fig. S1 below, we show the limiting value of the shear modulus (orange dots in lowest row) in the presence of weak interactions, namely $G(\gamma_c, \kappa \rightarrow 0^+)$, demonstrating once again the singular nature of the κ -perturbation represented by U_{weak} . We further elaborate on this point below.

S-III. THE GEOMETRIC OPERATOR AND STATES-OF-SELF-STRESS

Consider a disordered network of edges and nodes, similar to that shown in Fig. 1 of the main text. States of self stress (SSS) are assignment of putative (scalar) edge-forces $\{f_{ij}\}$ such that, for each node i

$$\sum_{\text{neighbors } j(i)} \mathbf{n}_{ji} f_{ij} = \mathbf{0}, \quad (\text{S1})$$

where \mathbf{n}_{ji} is the unit vector pointing from node j to node i , the sum runs over neighbors j connected *by an edge* to node i , and we choose the convention that positive (negative) f_{ij} 's represent compressive (tensile) forces. Generally, an isotropic disordered network must have $z \geq 2d$ for at least one SSS to exist; however, floppy networks with $z < 2d$ can develop a SSS, as indeed happens in the strain-stiffening problem.

At this point, it is convenient to adopt a bra-ket notation; in this notation, Eq. (S1) takes the form

$$\mathcal{S}^T |f\rangle = |0\rangle, \quad (\text{S2})$$

where the operator \mathcal{S} represents the geometry of the network. It is defined as

$$\mathcal{S}_{ij,k} = \frac{\partial r_{ij}}{\partial \mathbf{x}_k} = (\delta_{jk} - \delta_{ik}) \mathbf{n}_{ij}, \quad (\text{S3})$$

where r_{ij} is the pairwise distance between nodes i, j , δ_{jk} is the Kronecker delta, \mathbf{x}_k is the position vector of the k 'th node, and $\mathbf{n}_{ij} \equiv (\mathbf{x}_j - \mathbf{x}_i)/r_{ij}$ is the unit vector pointing from node i to node j . For convenience, we define the concatenated operator $\mathcal{S}\mathcal{S}^T$ such that SSS correspond to its eigenmodes associated with zero eigenvalues, denoted here and in what follows by λ .

S-1. The variation $\delta\lambda(\kappa)$

In the absence of bending energy (corresponding to $\kappa = 0$), strain-stiffened networks feature a single SSS at the critical strain γ_c . We denote this SSS by $|\phi\rangle$ (note that above, a general SSS was denoted by $|f\rangle$), and recall that $\mathcal{S}^T |\phi\rangle = |0\rangle$; how does this SSS break down under the introduction of bending energy into the network? Let us assume that by introducing bending energies of order κ , the nodes undergo displacements \mathbf{u}_* (of typical magnitude $u_*(\kappa)$, see Fig. 1 in the main text). How does $\lambda = \langle \phi | \mathcal{S}\mathcal{S}^T | \phi \rangle$ — where \mathcal{S} is defined only on the stiff subsystem — change under node-displacements \mathbf{u}_* ? Denoting by $\delta\mathcal{S}$, $\delta\lambda$ and $|\delta\phi\rangle$ the variations of \mathcal{S} , λ and $|\phi\rangle$ under the displacements \mathbf{u}_* , respectively, we obtain to first order $\delta\lambda = 2\langle \phi | \mathcal{S}\mathcal{S}^T | \delta\phi \rangle + 2\langle \phi | \delta\mathcal{S}\mathcal{S}^T | \phi \rangle = 0$, because $\mathcal{S}^T |\phi\rangle = |0\rangle$. The next order,

which involves contributions of the form $\langle \phi | \delta \mathcal{S} \delta \mathcal{S}^T | \phi \rangle$ does not vanish, hence we conclude that to leading order we have

$$\delta \lambda \sim u_\star^2 \sim \kappa^{2/3}, \quad (\text{S4})$$

in agreement with our numerical tests presented in Fig. 2c of the main text.

S-IV. LINEAR AND FIRST NONLINEAR SHEAR MODULI

For any a solid (i.e. a system having a finite shear modulus) at zero temperature, given a potential energy U , the athermal linear shear modulus reads [S6]

$$G = G_{\text{Born}} - \mathbf{F}_\gamma \cdot \mathbf{H}^{-1} \cdot \mathbf{F}_\gamma, \quad (\text{S5})$$

where $G_{\text{Born}} \equiv V^{-1} \partial^2 U / \partial \gamma^2$ is the affine contribution to the shear modulus (which is regular), $\mathbf{F}_\gamma \cdot \mathbf{H}^{-1} \cdot \mathbf{F}_\gamma$ is the relaxation term that accounts for the softening due to non-affine displacements, $\mathbf{F}_\gamma \equiv -\frac{\partial^2 U}{\partial \mathbf{x} \partial \mathbf{x}}$ are the forces that emerge from applying an affine deformation, $\mathbf{H} \equiv \frac{\partial^2 U}{\partial \mathbf{x} \partial \mathbf{x}}$ is the Hessian matrix of the potential energy, and γ parametrizes the strain tensor $\boldsymbol{\epsilon}$ as

$$\boldsymbol{\epsilon} = \frac{1}{2} \begin{pmatrix} 0 & \gamma \\ \gamma & \gamma^2 \end{pmatrix}. \quad (\text{S6})$$

It has been shown [S7] that the shear modulus of a relaxed Hookean spring network at $U=0$, in which all spring stiffnesses are set to unity, is given by

$$G = \frac{1}{V} \sum_{\text{sss } \ell} \langle \phi_\ell | \frac{\partial r}{\partial \gamma} \rangle^2, \quad (\text{S7})$$

where $|\phi_\ell\rangle$ is the ℓ^{th} SSS, and $|\frac{\partial r}{\partial \gamma}\rangle$ is a vector in which each component corresponds to the derivative $\partial r_{ij} / \partial \gamma$, with r_{ij} denoting the pairwise distance pertaining to a particular edge i, j of the network. Isotropic, underconstrained (hypostatic) networks feature no SSSs, and thus $G=0$ as observed. Anisotropic strain-stiffened networks, however, feature a single SSS $|\phi\rangle$ at the critical strain γ_c . The latter state features a finite coupling to the strain that scales with the system size as $\langle \phi | \frac{\partial r}{\partial \gamma} \rangle^2 \sim N$ (with a z -dependent prefactor [S8], and notice that we adopt the convention $\langle \phi | \phi \rangle = 1$). Consequently, strain-stiffened networks feature an intensive shear modulus of order $G \sim \mathcal{O}(1)$ in the absence of bending energy ($\kappa=0$, and recall that the fibers stretching/compression stiffness has been set to unity).

How does the shear modulus G of critical states ($\gamma = \gamma_c$) change upon introducing the weak interactions U_{weak} featuring stiffnesses and forces of order κ ? We consider Eq. (S5) and first point out that while G_{Born} is regular [S6], the second term in Eq. (S5) — containing a full contraction of the *inverse* of the Hessian \mathbf{H}^{-1} — can be singular by virtue of low-lying vibrational modes of \mathbf{H} . We review the vibrational spectrum of strain-stiffened networks next.

S-1. Vibrational spectrum at the critical state

Consider first the $\kappa=0$ case, namely in the absence of soft bending energies. Strain-stiffened networks at $\gamma=\gamma_c$ are expected to have $\sim N(2d-z)$ zero modes, since we consider underconstrained networks with $z < 2d$. Zero modes are putative displacements $\boldsymbol{\Psi}$ that satisfy

$$\mathbf{n}_{ij} \cdot (\boldsymbol{\Psi}_j - \boldsymbol{\Psi}_i) = 0, \quad (\text{S8})$$

for all (stiff) springs connecting pairs of nodes i, j . The above equation tell us that zero modes in $\kappa=0$ networks do not stretch nor compress any of the (stiff) springs. At the strain-stiffening transition the energy is vanishingly small, therefore the Hessian takes the form

$$\mathbf{H}_{kl}(\gamma_c, \kappa=0) = \sum_{\text{springs } i, j} \Lambda_{ij, kl} \mathbf{n}_{ij} \otimes \mathbf{n}_{ij}, \quad (\text{S9})$$

where $\Lambda_{ij, kl} \equiv (\delta_{jk} - \delta_{ik})(\delta_{j\ell} - \delta_{i\ell})$, \otimes represents an outer (dyadic) product, and we take the stiffness of the stiff springs to be unity.

Once the soft interactions are introduced to the $\kappa=0$ strain-stiffened network, and after the minimization of the total energy $U=U_{\text{stiff}}+U_{\text{weak}}$ during which nodes are displaced a typical distance u_* , forces of order $f_{\text{stiff}} \sim \kappa^{2/3}$ emerge in the stiff sub-network, as explained in the main text (see discussion preceding Eq. (4) in the main text). The Hessian now assumes the form

$$\mathcal{H}_{k\ell}(\gamma_c, \kappa) = \left[\sum_{\text{stiff springs } i,j} \Lambda_{ij,k\ell} \mathbf{n}_{ij} \otimes \mathbf{n}_{ij} - \sum_{\text{stiff springs } i,j} \Lambda_{ij,k\ell} \frac{f_{ij}}{r_{ij}} (\mathcal{I} - \mathbf{n}_{ij} \otimes \mathbf{n}_{ij}) \right] + \mathcal{H}_{\text{soft}} \equiv \mathcal{H}_1 + \mathcal{H}_2 + \mathcal{H}_{\text{soft}}, \quad (\text{S10})$$

where $\mathcal{H}_{\text{soft}} \equiv \frac{\partial^2 U_{\text{soft}}}{\partial \mathbf{x} \partial \mathbf{x}} \sim \kappa$. What frequency do the zero modes Ψ in the $\kappa=0$ (critical) network at γ_c acquire in the perturbed, $\kappa > 0$ network? Employing standard degenerate perturbation theory (see e.g. [S9]), the new frequencies squared are eigenvalues of the matrix

$$\tilde{\mathcal{H}}_{\ell m} \equiv \Psi^{(\ell)} \cdot \delta \mathcal{H} \cdot \Psi^{(m)} = \Psi^{(\ell)} \cdot (\delta \mathcal{H}_1 + \delta \mathcal{H}_2) \cdot \Psi^{(m)} + \mathcal{O}(\kappa), \quad (\text{S11})$$

where $\delta \mathcal{H} = \mathcal{H}(\kappa) - \mathcal{H}(\kappa=0)$, and $\Psi^{(\ell)}, \Psi^{(m)}$ are degenerate zero modes of the unperturbed network. Since

$$\delta \mathbf{n}_{ij} = \frac{\partial \mathbf{n}_{ij}}{\partial \mathbf{x}} \cdot \mathbf{u}_*, \quad (\text{S12})$$

then

$$\Psi^{(\ell)} \cdot \delta \mathcal{H}_1 \cdot \Psi^{(m)} \sim u_*^2 \sim \kappa^{2/3}. \quad (\text{S13})$$

Next, since the forces in the stiff, perturbed network scale as $f_{\text{stiff}} \sim \kappa^{2/3}$, then also

$$\Psi^{(\ell)} \cdot \delta \mathcal{H}_2 \cdot \Psi^{(m)} \sim f_{\text{stiff}} \sim \kappa^{2/3}. \quad (\text{S14})$$

We conclude that the characteristic scale ω_κ of the newly acquired frequencies of the soft modes in the perturbed network is dominated by the stiff subsystem, and follows

$$\omega_\kappa \sim \kappa^{1/3}. \quad (\text{S15})$$

Assuming that, in the perturbed system, the two terms \mathcal{H}_1 and \mathcal{H}_2 contribute equally to the frequencies ω_κ of soft modes Ψ , one then expects that for stiff springs connecting nodes i and j

$$\mathbf{n}_{ij} \cdot (\Psi_j - \Psi_i) \sim \omega_\kappa \sim \kappa^{1/3}. \quad (\text{S16})$$

This scaling with frequency of radial projections of soft mode resembles that found in other jamming problems, see e.g. [S10].

S-2. Relaxation term of the shear modulus

With the results in Eqs. (S15) and (S16) at hand, we are now in position to analyze the relaxation term of the shear modulus (the second term in the RHS of Eq. (S5)). Using the eigenbasis of the Hessian $\{\Psi^{(\ell)}\}_{\ell=0}^{N_d}$, and their associated eigenvalues ω_ℓ^2 , we write

$$\mathbf{F}_\gamma \cdot \mathcal{H}^{-1} \cdot \mathbf{F}_\gamma = \sum_\ell \frac{(\mathbf{F}_\gamma \cdot \Psi^{(\ell)})^2}{\omega_\ell^2}. \quad (\text{S17})$$

This sum could be dominated by the soft modes Ψ (which were *zero* modes in the unperturbed, $\kappa=0$ network), with associated frequencies $\omega_\kappa \sim \kappa^{1/3}$. Notice, however, that \mathbf{F}_γ is dominated by the stiff potential U_{stiff} , and so we can write

$$(\mathbf{F}_\gamma)_i \simeq \sum_{\text{stiff neighbors } j(i)} \frac{\partial r_{ij}}{\partial \gamma} \mathbf{n}_{ji}, \quad (\text{S18})$$

or, in our bra-ket notation (and see Eq. (S3))

$$|F_\gamma\rangle = \mathcal{S}^T |\frac{\partial r}{\partial \gamma}\rangle, \quad (\text{S19})$$

where, once again, \mathcal{S} is only defined on the stiff subsystem. Following Eq. (S19), the overlaps squared $(\mathbf{F}_\gamma \cdot \Psi)^2$ for soft modes Ψ can be written as

$$(\mathbf{F}_\gamma \cdot \Psi)^2 = \langle \frac{\partial r}{\partial \gamma} | \mathcal{S} | \Psi \rangle^2 \sim \omega_\kappa^2 \sim \kappa^{2/3}, \quad (\text{S20})$$

and notice we have used Eq. (S16), namely that $\langle \Psi | \mathcal{S}^T \mathcal{S} | \Psi \rangle \sim \kappa^{2/3}$. We conclude from this discussion that the contribution of soft modes Ψ to the relaxation term of the shear modulus G follows

$$\frac{(\mathbf{F}_\gamma \cdot \Psi)^2}{\omega_\kappa^2} \sim \frac{\kappa^{2/3}}{\kappa^{2/3}} \sim \mathcal{O}(1). \quad (\text{S21})$$

Finally, these considerations lead us to expect that $G \sim \kappa^0$, as indeed shown in Fig. 3a of the main text. The above results also explain why the shear modulus jumps discontinuously from $\kappa \rightarrow 0^+$ to $\kappa = 0$, as shown in Fig. S1 above, as well as in the main text.

S-3. The first nonlinear shear modulus

The first nonlinear shear modulus $dG/d\gamma$ can be shown to consist of 4 terms containing zero, one, two, and three contractions of the *inverse* of the Hessian \mathcal{H}^{-1} [S11]. The most singular of these terms can be expressed via the eigenbasis of the Hessian as [S12]

$$\frac{dG}{d\gamma} \simeq \frac{1}{V} \sum_{\ell mn} \frac{(\Psi_\ell \cdot \mathbf{F}_\gamma)(\Psi_m \cdot \mathbf{F}_\gamma)(\Psi_n \cdot \mathbf{F}_\gamma) (\mathcal{U}''' \cdot \cdot \cdot \Psi_\ell \Psi_m \Psi_n)}{\omega_\ell^2 \omega_m^2 \omega_n^2} + \mathcal{O}(\mathcal{H}^{-2}), \quad (\text{S22})$$

where $\mathcal{U}''' \equiv \frac{\partial^3 U}{\partial \mathbf{x} \partial \mathbf{x} \partial \mathbf{x}}$ is the rank-3 tensor of derivatives of the potential with respect to coordinates \mathbf{x} , and $\cdot \cdot \cdot$ denotes a triple contraction. In order to resolve the κ -scaling of $dG/d\gamma$, we are left with analyzing the contribution of soft modes Ψ to $dG/d\gamma$, and in particular the full contractions

$$\mathcal{U}''' \cdot \cdot \cdot \Psi \Psi \Psi \sim \mathcal{U}'''|_{\kappa=0} \cdot \cdot \cdot \Psi \Psi \Psi + \frac{\partial^4 U}{\partial \mathbf{x} \partial \mathbf{x} \partial \mathbf{x} \partial \mathbf{x}} \Big|_{\kappa=0} \cdot \cdot \cdot u_* \Psi \Psi \Psi \sim u_* \sim \kappa^{1/3}, \quad (\text{S23})$$

where $\cdot \cdot \cdot$ denotes a quadruple contraction, and notice that $\mathcal{U}'''|_{\kappa=0} \cdot \cdot \cdot \Psi \Psi \Psi$ is expected to be very small from stability considerations, as explained in the main text. Together with the previously established scaling of the overlaps $\Psi \cdot \mathbf{F}_\gamma \sim \kappa^{1/3}$ (see Eq. (S20) above), the scaling of the soft frequencies $\omega_\kappa \sim \kappa^{1/3}$ (see Eq. (S15) above), and the form of Eq. (S22), we conclude that

$$\frac{dG}{d\gamma} \sim \kappa^{-2/3}, \quad (\text{S24})$$

as indeed shown in Fig. 3b of the main text.

S-V. NON-AFFINE DISPLACEMENTS OF STRAIN-STIFFENED NETWORKS

The non-affine displacements squared can be written using the eigenbasis decomposition of the Hessian as [S11]

$$u_{\text{n.a.}}^2 = \sum_\ell \frac{(\mathbf{F}_\gamma \cdot \Psi_\ell)^2}{\omega_\ell^4} \sim \frac{\kappa^{2/3}}{\kappa^{4/3}} \sim \kappa^{-2/3}, \quad (\text{S25})$$

where we have again used Eqs. (S15) and (S20) for soft modes Ψ and their associated eigenfrequencies ω_κ . This prediction is in very good agreement with the numerical simulations of [S13], as also mentioned in the main text. In the context of [S13], we note that under overdamped conditions (mimicking fluid-immersed networks), we expect the excess viscosity of the system (i.e. the viscosity on top of that of the surrounding fluid) to scale with the non-affine displacements squared $u_{\text{n.a.}}^2$, as argued in [S14, S15].

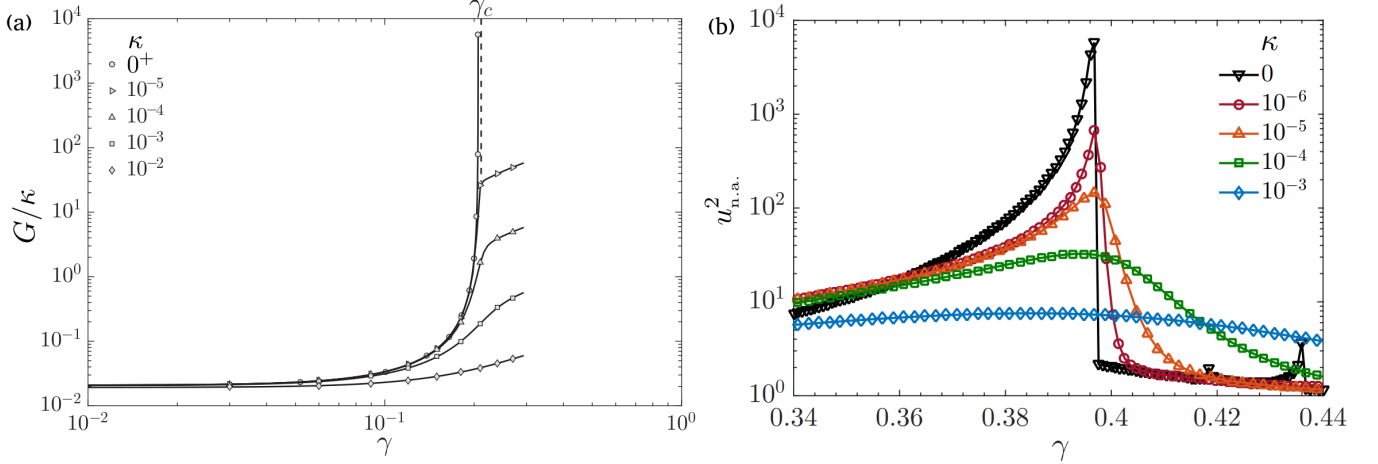


FIG. S2. (a) Adapted from [S8]. The shear modulus G — expressed in terms of the soft stiffness κ — is plotted against the shear strain γ . Here G was measured in packing-derived disordered networks with soft bending energies of stiffness κ , for various values of κ . The $\kappa \rightarrow 0^+$ data is generated using the geometric formalism introduced in [S8], and see further details therein. The strain scale $\delta\gamma_*(\kappa)$ can be seen as the strain at which the finite- κ signals depart from the $\kappa \rightarrow 0^+$ signal. (b) Adapted from [S8]. The non-affine displacements squared (cf. Eq. (S25)) are plotted against the shear strain γ , across the strain stiffening transition. Here measurements were performed in diluted honeycomb lattices with $z=2.73$, see further details in [S4].

S-VI. PREVIOUS NUMERICAL EVIDENCE FOR THE EXISTENCE OF $\delta\gamma_*(\kappa)$

In Fig. S2 above we reproduce Fig. 1 from [S8] (panel (a)) and Fig. 5.3 from [S4] (panel (b)), indicating the existence of a strain scale $\delta\gamma_*(\kappa)$ that vanishes as $\kappa \rightarrow 0^+$, both at strains below the critical strain, $\gamma < \gamma_c$ (panel (a)), and at strains above the critical strain, $\gamma > \gamma_c$ (panel (b)). See further details in the figure caption.

[S1] G. Kapteijns, E. Bouchbinder, and E. Lerner, Unified quantifier of mechanical disorder in solids, *Phys. Rev. E* **104**, 035001 (2021).

[S2] E. Bitzek, P. Koskinen, F. Gähler, M. Moseler, and P. Gumbsch, *Phys. Rev. Lett.* **97**, 170201 (2006).

[S3] M. F. J. Vermeulen, A. Bose, C. Storm, and W. G. Ellenbroek, *Phys. Rev. E* **96**, 053003 (2017).

[S4] R. Rens, *Theory of rigidity transitions in disordered materials* (PhD thesis, Univeristy of Amsterdam, the Netherlands, 2019).

[S5] M. Merkel, K. Baumgarten, B. P. Tighe, and M. L. Manning, *Proc. Natl. Acad. Sci. U.S.A.* **116**, 6560 (2019).

[S6] J. F. Lutsko, *J. Appl. Phys.* **65**, 2991 (1989).

[S7] M. Wyart, *Ann. Phys. Fr.* **30**, 1 (2005).

[S8] R. Rens, C. Villarroel, G. Düring, and E. Lerner, *Phys. Rev. E* **98**, 062411 (2018).

[S9] E. Bouchbinder and E. Lerner, Universal disorder-induced broadening of phonon bands: from disordered lattices to glasses, *New J. Phys.* **20**, 073022 (2018).

[S10] H. Mizuno, K. Saitoh, and L. E. Silbert, Elastic moduli and vibrational modes in jammed particulate packings, *Phys. Rev. E* **93**, 062905 (2016).

[S11] S. Karmakar, E. Lerner, and I. Procaccia, *Phys. Rev. E* **82**, 026105 (2010).

[S12] H. G. E. Hentschel, S. Karmakar, E. Lerner, and I. Procaccia, *Phys. Rev. E* **83**, 061101 (2011).

[S13] J. L. Shivers, A. Sharma, and F. C. MacKintosh, *arXiv preprint arXiv:2203.04891* (2022).

[S14] E. Lerner, G. Düring, and M. Wyart, *Proc. Natl. Acad. Sci. U.S.A.* **109**, 4798 (2012).

[S15] G. Düring, E. Lerner, and M. Wyart, *Phys. Rev. E* **89**, 022305 (2014).